Multivariable Model Predictive Control for a Virtual Synchronous Generation-Based Current Source Inverter

Jonggrist Jongudomkarn
Department of Electrical Engineering, Faculty of Engineering, Khon Kaen University, Thailand
Email: jongjo@kku.ac.th

Abstract—**Three-phase current-source inverters are an alternative solution for interfacing photovoltaic modules to the utility thanks to its voltage boosting ability. This paper presents a virtual synchronous generator strategy for a three-phase current-source inverter using a multivariable model predictive control. The proposed method can ensure operations in both grid-connected and islanded modes while achieving virtual inertia features to stabilize the grid frequency and active damping to reduce grid current distortions caused by an output CL filter included on the grid side of the system. The obtained simulation results in the PSCAD/EMTDC environment software verify the effectiveness and the excellent performance of the proposed method.**

Index Terms—**Current source inverter, distributed power generations, photovoltaics, power system stability, predictive control, virtual synchronous generator**

I. Introduction

The indiscriminate uses of fossil fuels to supply indefinite demand of the world's energy have led to the rapid depletion of these non-renewable resources. Furthermore, their exploitation is also believed to be the leading cause of global warming and climate change [1]. Thus, it was clear to power engineers and researchers that new ways to generate energy with low emissions and sustainable methods are imperative. A possible solution to this issue lies in the use of renewable energy sources (RES). Among these RES, photovoltaic (PV) energy has become a promising resource [2] for a grid-connected utilization because it offers high return-on-investment. Conventionally, PV-based distributed generators (DGs) are based on the voltage source inverter (VSI) topology. For such a system, the input DC voltage must be higher than the peak grid voltage. Hence, a DC-DC converter is usually included in the system's first stage to boost the input DC voltage, thus increasing the overall circuit complexity. An alternative way to achieve DC-AC inversion is a one-power-stage topology of a Current Source Inverter (CSI), as proposed in [3]–[6]. CSIs offer considerable advantages over the VSIs because they neither require second-order filters such as LLC or LCL at the output side, nor is it necessary to use additional converters to boost the dc voltage.

However, some issues still exist in the relevant control structure of CSI that must be resolved appropriately. For instance, a CL filter has to be inserted on the AC side of the CSI to reduce current distortions. However, this CL filter may cause oscillation in the output currents due to the resonance, especially in transient conditions, as reported in [7] and [8]. Passive damping or active damping methods must be included in the system to prevent this. Generally, the latter is preferable because it does not inflict further losses to the system and can be integrated directly into the controller, as studied in [5], [7], and [8]. Apart from that, the existing control schemes [9]–[11] for grid-connected CSI-based DGs are current-controlled, for which the maximum power extracted from the RES is always injected into the grid. This control paradigm is subtle as long as the DGs are operating in normal conditions. However, when a fault occurs in the grid, the system will be islanded. In this condition, the DGs are incapable of delivering the power to the local load if the controllers do not regulate the voltage and the frequency. Although a voltage-controlled method for CSI were proposed in some woks, e.g. [6], it cannot operate in grid-connected mode. Furthermore, the conventional control methods have neither a prime mover nor rotating inertia. Therefore they do not contribute to the stabilization of the grid frequency. One of the highly-rated solutions to prevent these problems is implementing a virtual synchronous generator (VSG). The past research works have demonstrated that the VSG-based DGs can solve issues related to frequency deviations and capable of islanded operation [12]–[16].

Over the last few years, finite control set model predictive control (FCS-MPC) has emerged as an attractive alternative for the control of power electronics applications since it offers several benefits, including simple multivariable control, the possible inclusion of constraints, straightforward control law, and fast dynamic response [17]. As for DGs, several control solutions based on FCS-MPC appeared in the literature [18]–[23].

Manuscript received September 10, 2020; revised October 25, 2020; accepted November 30, 2020.

Corresponding author: Jonggrist Jongudomkarn (email: jongjo@kku.ac.th).

doi: 10.18178/ijeetc.10.3.196-202

In the previous works of the author [21]–[23], the multivariable FCS-MPC-based VSG for a VSI and an indirect boost matrix converter (IBMC) shows high compatibility between the FCS-MPC and VSG. In addition to integrating the inertia support feature, the FCS-MPC-based control scheme utilizes a simultaneous control of both voltage and current of the output *LCL*-filter to provide active damping of the resonant energy oscillation between the filter inductor and the filter capacitor. The mentioned oscillation will occur if either filter voltage or the filter current is solely controlled. This performs an alternative method to damp the filter resonance without a dedicated active damping part in the control algorithm [22]–[26].

This paper proposes the multivariable FCS-MPC-based VSG control for a three-phase CSI-based DG. The proposed control strategy is explained in detail, including the models used for voltage and current prediction, the cost function used for current vector selection, and the VSG control. Thanks to adopting the VSG strategy, the proposed control scheme displays the ability to operate in both grid-tied and islanded modes, while the controller is also capable of providing the inertial power to stabilize the grid frequency. Furthermore, the multivariable control of capacitor voltage and inductor current of the output CL-filter provides active filter resonance damping. Results obtained from the PSCAD/EMTDC software environment are presented to exhibit the proposed strategy's performance.

II. Description of the System Model

A. System Model

A topology of the system under study is illustrated in Fig. 1. The inverter consists of six power transistor switches. The six switches have series diodes for forming a rear-end current source inverter (CSI). Throughout the operation, the CSI must have at least one of the upper switches and one of the lower switches conducting to ensure a current path for the DC-current. The number of possible switching states that the inverter can generate is limited. For active vectors denoted as I_1–I_6, the current source converter uses six unidirectional switches in two converter's legs: one in the upper part (switches 1, 2, 3) and the second in the lower part of the bridge (switches 4, 5, 6). The switches are chosen in such a way, as concluded in Fig. 1. Three passive vectors (zero vectors) are denoted as I_7–I_9. In this case, both upper and lower switches of one of the three converter's legs are turned on at the same time.

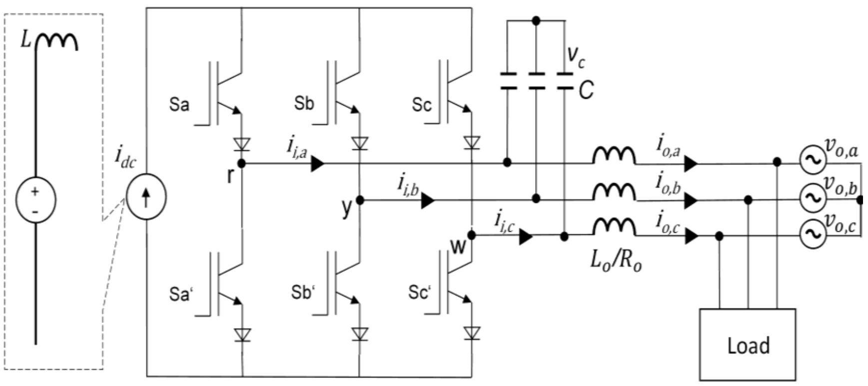

Fig. 1. Topology of the CSI-based DG.

B. Filter Resonance

The main objective of the grid-connected CSI-based DG is to control the current vector components that are injected into the grid. Although the use of a CL filter has a positive effect on improving the quality of the grid current, attention is required regarding the presence of the resonance frequency f_{res} of a CL filter described by the following relationship:

$$f_{\text{res}} = \frac{1}{2\pi}\frac{1}{\sqrt{L_o C}} \tag{1}$$

where L_o is the filter inductance, and C is the filter capacitance. The conventional control methods for CSI [3]–[6] are based on current-controlled. For such control systems, the control algorithm uses inverter current i_{inv} to control the output current i_0 indirectly. In this case, the transfer function of the CL filter is expressed with (2).

It can be observed from (2) that if there are harmonics related to the resonance frequency f_{res}, they will be amplified by the gain of the output filter, causing the resonance to occur between the grid-side inductor L_o and the filter capacitor C. This is crucial for the control system because the harmonics related to the resonance frequency are generated in transient conditions, as reported in [7] and [8]. The highly-rated solutions to this problem are active damping methods based on a virtual resistor, as studied in [7] and [8]. However, this resonance can also be avoided using the simultaneous control of capacitor voltage and inductor current of the output CL-filter, as will be shown later in the paper.

$$G(s) = \frac{i_o(s)}{i_{\text{inv}}(s)} = \frac{1}{1 + L_o C s^2} = \frac{1}{1 + s^2/\omega_{\text{res}}} \tag{2}$$

III. Proposed Control of the System

A. Virtual Synchronous Generator Control

The VSG control's main task is to track the dispatch power command while providing inertial power to the grid to help stabilize the grid frequency. This can be realized with the structure of a VSG control shown in Fig. 2. It consists of "Swing Equation Function", "Governor", and "Q droop" blocks. The P_o, P_{out}, P_{gov}, Q_o, Q_{out}, V_{out}, ω_m, ω_{PLL}, E^*, and θ^* variables in the control diagram represent the output active power command, the output active power, the shaft power from the governor, the output reactive power command, the output reactive power, the output voltage amplitude, the mechanical frequency of rotors, the output frequency measured by PLL, the voltage reference magnitude, and the power angle reference, respectively. Virtual inertia is emulated in the block "Swing Equation Function" with the well-known swing equation:

$$P_{\text{gov}} - P_{\text{out}} + D(\omega_m - \omega_g) = J\omega_m \frac{d\omega_m}{dt} \tag{3}$$

where D is the damping factor produced by the damper windings, J is the moment of inertia, P_{out} is the output active power, ω_m is the virtual rotor angular frequency, and ω_g is the grid frequency. The function of the shaft power P_{gov} regulated by a governor is given as

$$P_{\text{gov}} = P_0 - k_p(\omega_m - \omega_{\text{base}}) \tag{4}$$

where k_p is the droop coefficient and ω_{base} is the nominal grid frequency. The block "Q droop", as well as the design details of all blocks in Fig. 2, and the tuning of the VSG parameters, are well explained in [16], and hence their explanations will be omitted in this work.

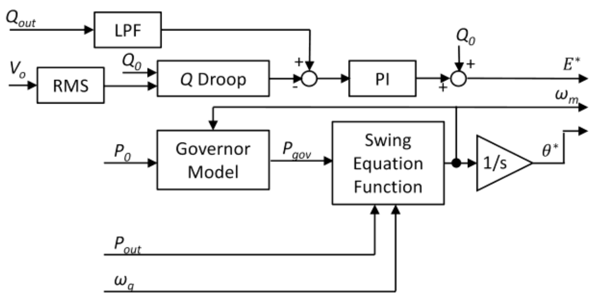

Fig. 2. Control diagram of the VSG control scheme.

B. Finite Set Model Predictive Control Design

In order to use MPC to forecast the future values of the system variables, the mathematical model of the system is required. Therefore, the model of the CSI used for the proposed control will be explained in this section.

First, to realize a DG that can operate in both grid-connected and islanded modes, the inverter output voltage and inverter current should be the variables to be controlled in the FCS-MPC for the CSI. Thus, the model of a three-phase CSI with output CL filter, as depicted in Fig. 1 is utilized to forecast the voltage and current outputs. This model can be described in $\alpha\beta$-frame using capacitor dynamics equation (5) and inductance dynamics equation (6):

$$C\frac{d\mathbf{v}_c}{dt} = \mathbf{i}_{\text{inv}} - \mathbf{i}_o \tag{5}$$

$$L_o\frac{d\mathbf{i}_o}{dt} = \mathbf{v}_c - \mathbf{v}_o \tag{6}$$

where $\mathbf{v}_c = [v_{c,\alpha}\ v_{c,\beta}]^T$, $\mathbf{v}_o = [v_{o,\alpha}\ v_{o,\beta}]^T$, $\mathbf{i}_{\text{inv}} = [i_{\text{inv},\alpha}\ i_{\text{inv},\beta}]^T$ and $\mathbf{i}_o = [i_{o,\alpha}\ i_{o,\beta}]^T$ are capacitor voltage, output voltage, inverter current, and the output current, respectively. These equations can be rewritten as follows:

$$\dot{\mathbf{x}} = \mathbf{A}\mathbf{x} + \mathbf{B}\mathbf{v}_o + \mathbf{B}_d\mathbf{i}_{\text{inv}} \tag{7}$$

where

$$\mathbf{x} = [i_{o,\alpha}\quad i_{o,\beta}\quad v_{c,\alpha}\quad v_{c,\beta}]^T$$

$$\mathbf{A} = \begin{bmatrix} 0 & 0 & \frac{1}{L_o} & 0 \\ 0 & 0 & 0 & \frac{1}{L_o} \\ -\frac{1}{C} & 0 & 0 & 0 \\ 0 & -\frac{1}{C} & 0 & 0 \end{bmatrix}$$

$$\mathbf{B} = \begin{bmatrix} -\frac{1}{L_o} & 0 & 0 & 0 \\ 0 & -\frac{1}{L_o} & 0 & 0 \end{bmatrix}^T, \ \mathbf{B}_d = \begin{bmatrix} 0 & 0 & \frac{1}{C} & 0 \\ 0 & 0 & 0 & \frac{1}{C} \end{bmatrix}^T$$

A discrete-time model of the system derived from (7), using the general forward-difference Euler formula, for a sampling time T_s can be expressed as

$$\mathbf{x}(k+1) = \mathbf{A}_q\mathbf{x}(k) + \mathbf{B}_q\mathbf{v}_o(k) + \mathbf{B}_{\text{dq}}\mathbf{i}_o(k) \tag{8}$$

where

$$\mathbf{A}_q = e^{\mathbf{A}T_s},\ \mathbf{B}_q = \int_0^{T_s} e^{\mathbf{A}\tau}\mathbf{B}d\tau,\ \mathbf{B}_{\text{dq}} = \int_0^{T_s} e^{\mathbf{A}\tau}\mathbf{B}_d d\tau .$$

From (7)–(8), it can be seen that the future values $\mathbf{v}_c(k+1)$ and $\mathbf{i}_o(k+1)$ can be determined according to inverter stage current $\mathbf{i}_{\text{inv}}(k)$. For each active current vectors (SC1-SC6) of CSI, the inverter stage current $\mathbf{i}_{\text{inv}}(k)$ is defined as

$$\mathbf{i}_{\text{inv}}(k) = [S_1 - S_4\quad S_2 - S_5\quad S_3 - S_6]^T i_{DC} \tag{9}$$

where S_1, S_2, S_3, S_4, S_5, and S_6, represent the switching states of the six switches in the inverter stage, as depicted in Fig. 1. The switching state's value consists of 1 and 0, for which it represents the closed and open states, respectively.

C. Current References and Resonances Damping

To ensure proper operations, the CSI requires a capacitive output filter. However, in order to improve the quality of the waveforms, CL-filter is usually preferred. Nevertheless, the presence of resonance frequency has to be considered. Since the FCS-MPC possesses a variable switching frequency, it might generate harmonics components at the resonant frequency of CL-filter at a specific operating point. However, this will result in resonance only if the output inverter current $\mathbf{i}_o(s)$ is directly controlled, whereas the capacitor voltage $\mathbf{v}_c(s)$, is indirectly controlled by the current and thus highly dependent on filter impedances, as described in (2).

The proposed FCS-MPC utilizes a multivariable system to control both $\mathbf{v}_c(s)$ and $\mathbf{i}_o(s)$ simultaneously. It is different from conventional cascade control of voltage and current, where the settling time of the inner loop must be significantly faster than the settling time of the outer loop. Therefore, at the resonant frequency where $\mathbf{v}_c(s)$ and $\mathbf{i}_o(s)$ are oscillating with the same dynamics, the control of the outer loop is not fast enough to provide a damping effect. Contrarily, the multivariable control of the FCS-MPC is conducted at the same bandwidth. This ensures that the regulation of $\mathbf{v}_c(s)$ can damp the distortion caused by the harmonics of $\mathbf{i}_o(s)$ and the control of $\mathbf{i}_o(s)$ can reduce the disturbance caused by the harmonics of $\mathbf{v}_c(s)$. Hence, by controlling CL-filter voltage and current at the same instances, the filter's frequency response is no longer influenced by its impedance alone. Thus the uncontrolled resonant energy oscillation between the inductances and the capacitance is effectively avoided, as will be proved later in the paper. This concept has also been successfully put in an application by the author in the FCS-MPC-based grid-connected VSI in [22] and in the FCS-MPC-based IBMC in [23], while similar concepts were also proposed in [24]–[26] for the grid-connected FCS-MPC-based AC/DC converter.

The voltage command for the FCS-MPC can be obtained from the VSG control scheme in Fig. 2. However, to achieve resonance damping, both voltage and current control must be embedded into a single loop control, as depicted in Fig. 3. Therefore, the current command must be provided for the FCS-MPC scheme. The current command can be determined by considering the relationship between the inverter output voltage, the output current, and the capacitor phase voltage shown in Fig. 1. It can be described in a stationary ($\alpha\beta$) frame as

$$\mathbf{v}_{c,\alpha\beta} = \mathbf{v}_{o,\alpha\beta} + \mathbf{i}_{o,\alpha\beta}(R_o + j(X_o)) \tag{10}$$

where $\mathbf{v}_{c,\alpha\beta}$ is the capacitor voltages, $\mathbf{i}_{o,\alpha\beta}$ the output current and $\mathbf{v}_{o,\alpha\beta}$ is the output voltages. X_o denotes the filter reactance and R_o denotes filter resistance. If we consider that the $\mathbf{v}_{c,\alpha\beta}$ in (10) equals the voltage command described by E^* and θ^* from the VSG control, the currents references i_α^* and i_β^* can be expressed as illustrated in (11), and they will be used as the current command for the CSI side of the FCS-MPC.

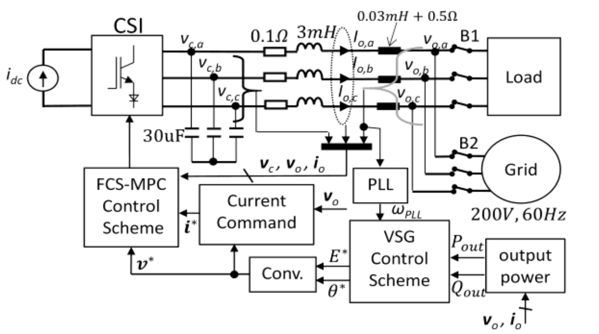

Fig. 3. Control diagram of the proposed FCS-MPC-based VSG control scheme.

$$\begin{bmatrix} i_\alpha^* \\ i_\beta^* \end{bmatrix} = \mathbf{Y}\left\{ \begin{bmatrix} E^*\cos\theta^* \\ E^*\sin\theta^* \end{bmatrix} - \begin{bmatrix} v_{o,\alpha} \\ v_{o,\beta} \end{bmatrix} \right\} \tag{11}$$

where

$$\mathbf{Y} = \frac{1}{R_o^{\,2} + X_o^{\,2}} \begin{bmatrix} R_o & X_o \\ -X_o & R_o \end{bmatrix}.$$

D. Cost Function Definition

Contrarily to classical control schemes, the cost function's presence allows the FCS-MPC to take into account a number of control goals and control different state variables simultaneously. Therefore, it is highly relevant to define the cost function properly. For the control of CSI, the control system is set to track the voltage and current references simultaneously. This can be achieved by defining a cost function as follows.

$$\begin{aligned} g_{\mathrm{CSI}} &= k_v\left(\mathbf{v}_{c,\alpha\beta,\mathrm{pu}}(k+1) - \mathbf{v}^*_{\alpha\beta,\mathrm{pu}}\right)^2 + \\ &\quad k_i\left(\mathbf{i}_{f,\alpha\beta,\mathrm{pu}}(k+1) - \mathbf{i}^*_{\alpha\beta,\mathrm{pu}}\right)^2 \end{aligned} \tag{12}$$

where $\mathbf{v}^*_{\alpha\beta} = [v^*_\alpha\ v^*_\beta]^T$ is the reference vector of the capacitor voltage, $\mathbf{i}^*_{\alpha\beta} = [i^*_\alpha\ i^*_\beta]^T$ is the reference vector of the inductor current, $\mathbf{v}_{c,\alpha\beta}(k+1) = [v_{c,\alpha?}v_{c,\beta}]^T$ is the predicted capacitor voltage and $\mathbf{i}_{f,\alpha\beta}(k+1) = [i_{f,\alpha}\ i_{f,\beta}]^T$ is the predicted inductance current, and the subscript *pu* indicates the per-unit value.

The selection of k_v and k_i is done according to the guideline provided by [27]. By evaluating the ability of the controller to synchronize with the grid and the quality of the active damping achieved by the weighting factors, the k_v:k_i the ratio of 1:4 is selected for the proposed control.

IV. Results and Discussion

In order to evaluate the performance of the proposed control scheme, simulation-based studies are performed in the PSCAD/EMTDC environment. The simulation parameters are given, as shown in Table I. The parameters indicated in Fig. 1 were respectively realized as follows, L_o=3mH, R_o=0.1Ω and C= 30μF. The filter inductances are designed such that the voltage drop across the inductor is around 0.08pu. The capacitance C is then calculated to set the filter's cut-off frequency much lower than the switching frequency. The sampling frequency for the CSI $f_{s,\mathrm{cst}}$ of the FCS-MPC-based control is selected at 20kHz, respectively. This brings about the measured average switching frequency around 10kHz for the FCS-MPC-based control.

TABLE I: CONTROL PARAMETERS

Parameters	Values	Parameters	Values
S_{base}	5 kVA	J	0.56kg·m^2
k_p	40 pu	D	200 pu
V_{base}	200 V	$f_{s,\mathrm{cst}}$	20 kHz
ω_{base}=ω_{grid}	376.99 rad/s		

A. Normal Operation

The proposed VSG control performance for the CSI is verified with simulations of the test circuit displayed in Fig. 2. Initially, the DG system is connected to the grid with the reference active power of DG (P_o) equals 5kW and reference reactive power of DG (Q_o) equals 0 var. The DG system is then set to operate in islanded mode at T = 7s. The load initially connected to the system during the islanded mode is 4kW, and it is increased to 6kW at T = 10s. The output voltage and current at the instance of the grid-islanding are illustrated in Fig. 4. The figure shows that the inverter can ride through the grid-islanding while producing sinusoidal waveforms of voltage and current in both grid-connected and islanded operation.

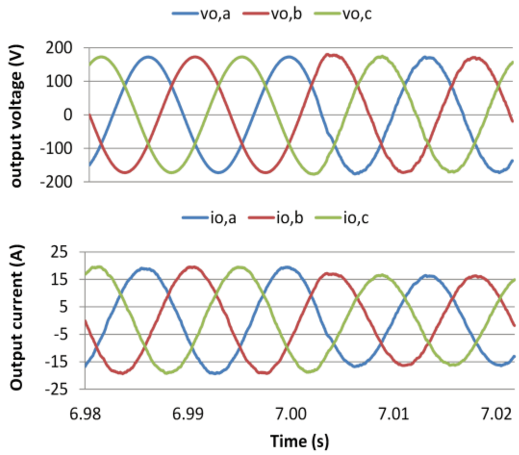

Fig.4. Output voltage and current waveforms during grid-islanding.

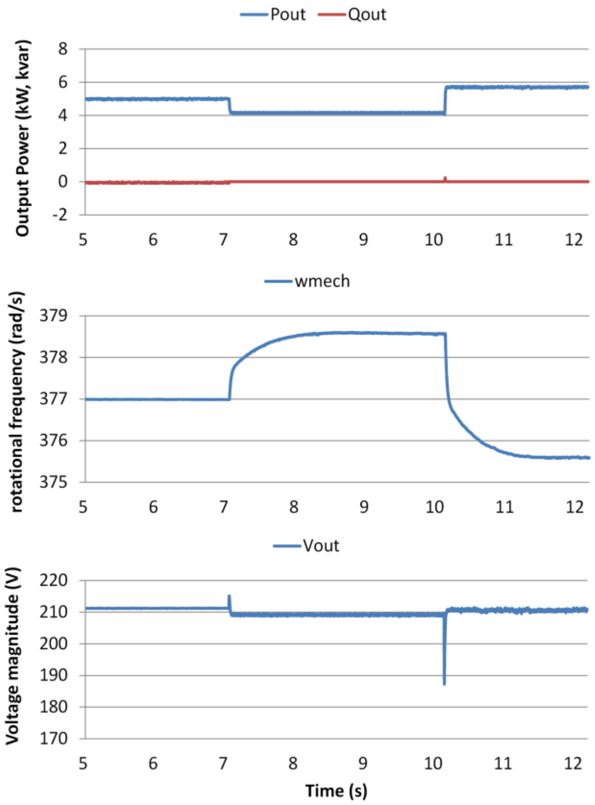

Fig. 5. Output active and reactive power, the output frequency, and the output voltage amplitude of the proposed control scheme, from top to bottom, respectively.

The output active and reactive powers, the output rotational frequency, and the output voltage magnitude for the whole simulation are illustrated in Fig. 5. It is shown that the system quickly and seamlessly commutates from the grid-connected mode into the islanded mode, supplying the required 4kW of power to the local load. The system can also react to change in load during islanded operation, as evidenced in Fig. 4 and Fig. 5. The output frequency and the output active power of the control system in Fig. 5, are illustrating how the system is settling to operate at a different frequency according to the droop characteristic, whereas the output voltage amplitude of the system is maintained slightly above the nominal value (V_{based}) throughout the operation to compensate for the voltage drop in the line impedance. Furthermore, the change in output frequency during the load transition in islanded mode demonstrates the controller's inertial response, as the output frequency slowly decreases from around 378.5 rad/s to around 375.5 rad/s. The reduction of frequency occurs for around 1 s until the new frequency set point is reached. This is a typical VSGs performance, as analyzed in [15] and [16].

B. Active Damping Ability

In order to verify the active damping ability, the simulations of the proposed control scheme are conducted under two different control parameters. In Case 1, the k_v is set to 0, while the k_i is set at 1. In this condition, only the output current ($\mathbf{i}_o$) is controlled through the control of inverter current ($\mathbf{i}_{\text{inv}}$), and the filter voltage is uncontrolled. In Case 2, the ratio of k_v:k_i is set to 1:4 to achieve the simultaneous control of filter voltage and output current. For both cases, the amplitude of current reference is set to increase from 1pu to around 1.25 pu at T = 5s, while the DG is operating in grid-connected mode. The current waveforms of Case 1 and Case 2 are illustrated in Fig. 6 (a) and Fig. 6 (b), respectively. It is clearly displayed in the figure that the distortion is more significant in case 1, where only $\mathbf{i}_o$ is controlled. The distortion is exceptionally substantial during the transient condition than in the steady-state condition because additional harmonics related to f_{res} are generated by the sudden change of current reference. In steady-state, on the other hand, harmonics related to f_{res} are smaller since they are only generated by the variable switching of the FCS-MPC scheme.

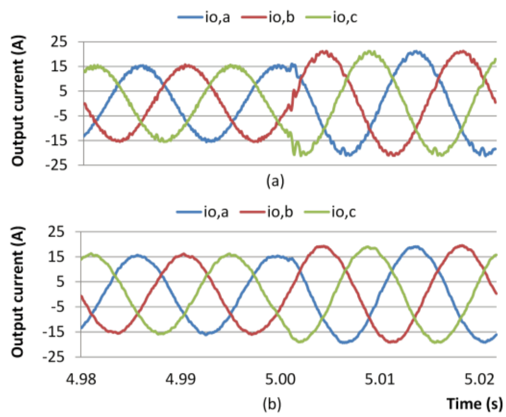

Fig. 6. Output current waveforms for (a) case 1 and (b) case 2.

It can be concluded from the simulation result that in Case 1, the harmonic components around f_{res} of the current is amplified by the transfer function of the CL filter (2), causing resonance and current distortions. In contrast to that, by controlling the output voltage and current simultaneously in case 2, the oscillation between capacitor and inductor is effectively avoided and hence even when there are the harmonic components around f_{res}, the gain of the transfer function (2) is no longer applied to these harmonic components.

V. Conclusion

The relevant existing control methods for CSI-based DG have shortcomings such as the incapability of both grid-connected and islanded operation, the lack of virtual inertia, and the generation of distorted output current in transient condition. To solve these problems, a novel control scheme based on multivariable FCS-MPC for the implementation of VSG is proposed in this paper. Simulation studies indicate that the proposed control scheme offers many advantages. For instance, thanks to the deployment of the proposed VSG control, the controller can provide the inertia property from the power source to support the grid frequency stability and is also capable of operating independently in islanded operation, maintaining the control of output voltage and output frequency actively. The utilization of multivariable control of voltage and current, grants the controller with active damping ability to damp the resonances caused by the output *CL* filter. The present work was an initial step to apply a VSG control in a CSI-based DG, and for future steps of this work, conducting experimental tests for evaluating and validating the proposed control strategy is considered.

Conflict of Interest

The authors declare no conflict of interest.

Author Contributions

The paper and all work were done by the author who approved the final version.

Acknowledgment

This work was supported by the faculty of engineering, Khon Kaen University, Thailand.

References

[1] B. Bose, "Global warming: Energy, environmental pollution, and the impact of power electronics," *IEEE Ind. Electron. Mag*., vol. 4, pp. 6-17, Mar. 2010.

[2] Global Market Outlook For Solar Power/2016-2020. [Online]. Available: https://resources.solarbusinesshub.com/solar-industry-reports/item/global-market-outlook-for-solar-power-2016-2020

[3] Y. Chen and K. Smedley, "Three-phase boost-type grid-connected inverter," *IEEE Trans. Power Electron*., vol. 23, no. 5, pp. 2301-2309, Sept. 2008.

[4] Q. Lei and F. Z. Peng, "Space vector pulsewidth amplitude modulation for a buck–boost voltage/current source inverter," *IEEE Trans. on Power Electronics*, vol. 29, no. 1, pp. 266-274, January 2014.

[5] C. Du, J. Zhou, and Y. Ma, "Predictive current control of a current-source inverter with active damping method," in *Proc. IEEE Energy Conversion Congress and Exposition (ECCE)*, Montreal, 2015, pp. 1100-1104.

[6] H. Feroura, F. Krim, B. Tabli, and A. Laib, "Finite-set model predictive voltage control for islanded three phase current source inverter," in *Proc. 5th Int. Conf. on Electrical Engineering - Boumerdes (ICEE-B)*, Boumerdes, 2017, pp. 1-5.

[7] M. Salo and H. Tuusa, "A vector controlled current-source PWM rectifier with a novel current damping method," *IEEE Trans. Power Electron*., vol. 15, no. 3, pp. 464-470, May 2000.

[8] P. A. Dahono, Y. R. Bahar, Y. Sato, and T. Kataoka, "Damping of transient oscillations on the output LC filter of PWM inverters by using a virtual resistor,"in *Proc. 4th IEEE Int. Conf. on Power Electronics and Drive Systems*, Denpasar, Indonesia, 2001, pp. 403-407.

[9] S. Sahoo, S. K. M ishra, and J. K. Sahu, "Standalone PV system integrated with hysteresis current controlled inverter using MPPT techniques," in *Proc. Int. Conf. on Communication and Electronics Systems (ICCES)*, Coimbatore, India, 2019, pp. 2024-2029.

[10] E. Lorenzani, G. Migliazza, F. Immovilli, and G. Buticchi, "CSI and CSI7 current source inverters for modular transformerless PV inverters," *Chinese Journal of Electrical Engineering*, vol. 5, no. 2, pp. 32-42, June 2019.

[11] A. Godlewska, "Finite control set model predictive control of current source inverter for photovoltaic systems,"in *Proc. 14th Selected Issues of Electrical Engineering and Electronics (WZEE)*, Szczecin, Poland, 2018, pp. 1-4.

[12] J. Driesen and K. Visscher, "Virtual synchronous generators," in *Proc. IEEE Power and Energy Society General Meeting - Conversion and Delivery of Electrical Energy in the 21st Century*, Pittsburgh, 2008, pp. 1-3.

[13] Q.-C. Zhong and G. Weiss, "Synchronverters: inverters that mimic synchronous generators," *IEEE Trans. Ind. Electron*., vol. 58, no. 4, pp. 1259–1267, Apr. 2011.

[14] S. D'Arco and J. A. Suul, "Virtual synchronous machines - classification of implementations and analysis of equivalence to droop controllers for microgrids," in *Proc. IEEE Grenoble Conf.*, Grenoble, 2013, pp. 1-7.

[15] J. Liu, Y. Miura and T. Ise, "Comparison of dynamic characteristics between virtual synchronous generator and droop control in inverter-based distributed generators," *IEEE Trans. on Power Electronics*, vol. 31, no. 5, pp. 3600-3611, May 2016.

[16] J. Liu, Y. Miura, H. Bevrani, and T. Ise, "Enhanced virtual synchronous generator control for parallel inverters in microgrids," *IEEE Trans. Smart Grid*, vol. 8, no. 5, pp. 2268–2277, Sep. 2017.

[17] J. Rodriguez, M. P. Kazmierkowski, J. R. Espinoza, *et al*., "State of the art of finite control set model predictive control in power electronics," *IEEE Trans. on Industrial Informatics*, vol. 9, no. 2, pp. 1003-1016, May 2013.

[18] B. Arif, L. Tarisciotti, P. Zanchetta, J. C. Clare, and M. Degano, "Grid parameter estimation using model predictive direct power control," *IEEE Trans. on Industry Applications*, vol. 51, no. 6, pp. 4614-4622, Nov.-Dec. 2015.

[19] J. Hu, J. Zhu, and D. G. Dorrell, "Model predictive control of inverters for both islanded and grid-connected operations in renewable power generations," *IET Renewable Power Generation*, vol. 8, no. 3, pp. 240-248, 2014.

[20] F. Donoso, A. Mora, R. Cárdenas, A. Angulo, D. Sáez, and M. Rivera, "Finite-set model-predictive control strategies for a 3L-NPC inverter operating with fixed switching frequency," *IEEE Trans. on Industrial Electronics*, vol. 65, no. 5, pp. 3954-3965, May 2018.

[21] J. Jongudomkarn, J. Liu, and T. Ise, "Virtual synchronous generator control with reliable fault ride-through capability by adopting model predictive control," in *Proc. Int. Power Electronics Conf.*, Niigata, 2018, pp. 3902-3909.

[22] J. Jongudomkarn, J. Liu, and T. Ise, "Virtual synchronous generator control with reliable fault ride-through ability: A

solution based on finite-set model predictive control," *IEEE Journal of Emerging and Selected Topics in Power Electronics*, vol. 8, no. 4, pp. 3811-3824, 2020.

[23] J. Jongudomkarn, J. Liu, Y. Yanagisawa, H. Bevrani, and T. Ise, "Model predictive control for indirect boost matrix converter based on virtual synchronous generator," *IEEE Access*, vol. 8, pp. 60364-60381, Mar. 2020.

[24] P. Falkowski and A. Sikorski, "Dead-time compensation in a new FCS-MPC of an AC/DC converter with a LCL filter," in *Proc. 13th Selected Issues of Electrical Engineering and Electronics (WZEE)*, Rzeszow, 2016, pp. 1-6.

[25] N. Panten, N. Hoffmann, and F. W. Fuchs, "Finite control set model predictive current control for grid-connected voltage-source converters with LCL filters: A study based on different state feedbacks," *IEEE Trans. on Power Electronics*, vol. 31, no. 7, pp. 5189-5200, July 2016.

[26] P. Falkowski and A. Sikorski, "Finite control set model predictive control for grid-connected AC–DC converters with LCL filter," *IEEE Trans. on Industrial Electronics*, vol. 65, no. 4, pp. 2844-2852, April 2018.

[27] P. Cortes, S. Kouro, B. L. Rocca, *et al*., "Guidelines for weighting factors design in model predictive control of power converters and drives," in *Proc. IEEE International Conf. on Industrial Technology*, Gippsland, VIC, 2009, pp. 1-7.

Jonggrist Jongudomkarn was born in Khon Kaen Thailand. He received the B.Eng. and Diplom-Ingenieur Univ. (M.Sc.) degrees in electrical engineering and information technology from the Technical University of Munich, Germany, in 2012 and 2013, respectively and received the Ph.D. degree in electrical engineering from Osaka University, Japan, in 2020. He is currently with the Faculty of Engineering Khon Kaen University, Thailand; His research interests include distributed generators, power quality, electric machine drives, and power conversion.